Bulk and Surface Simulation Studies of $La_{1-x}Ca_xMnO_3$

M. Javed Akhtar,*[,†,‡] C. Richard A. Catlow,[†] Ben Slater,[†] Andrew M. Walker,[†,§] and Scott M. Woodley*[,†]

Davy Faraday Research Laboratory, The Royal Institution of Great Britain, 21 Albemarle Street, London W1S 4BS, United Kingdom, Pakistan Institute of Nuclear Science and Technology, P.O. Nilore, Islamabad, Pakistan, and Research School of Earth Sciences, The Australian National University, Mills Road, Canberra, ACT 0200, Australia

Received October 12, 2005. Revised Manuscript Received December 23, 2005

The structural properties of $La_{1-x}Ca_xMnO_3$ are investigated by employing bulk and surface simulation techniques. The potential parameters reproduce the crystal structures of both end compositions, giving good agreement with experimental data. The calculated variation of the lattice parameters with Ca concentration also agrees with experimental values. Our calculations predict the formation of a solid solution and that, at very low temperatures and near $x = {}^1/_2$, the cations preferentially order on both A and B sites. The driving mechanism for cation ordering arises from both the coulomb and ion-size terms, with the relative proportions depending on composition. However, at temperatures where high-temperature synthesis normally occurs, the ordering of the cations is random. Surface energies are calculated for (010) and (110) surfaces for the end compositions: in $LaMnO_3$, Mn-terminated layers are more stable, whereas Ca-terminated layers are found to be more stable for the $CaMnO_3$ system. It is proposed that the surface structure of intermediate compositions is controlled by a subtle interplay between the different cation ionic strengths and their respective concentrations.

Introduction

The discovery of colossal magnetoresistance (CMR) in $La_{1-x}Ca_xMnO_3$ and related manganese-based perovskite compounds has generated considerable interest in these materials.[1−2] In addition, numerous studies have been reported in which other dopants are introduced at both La and Mn sites.[3−9] The end compositions, $LaMnO_3$ and $CaMnO_3$, are antiferromagnetic insulators. However, partial substitution of La with Ca strongly influences the electronic and magnetic properties of the materials. The $La_{1-x}Ca_xMnO_3$ system becomes a ferromagnetic metal in the intermediate composition range $0.1 < x < 0.6$. The doping level and stoichiometry play an important role in controlling the nature of the magnetic and electron-transport properties, with small changes in the concentration of the dopant having pronounced effects.[10] Indeed, in the intermediate-doping regime (typically near $x = 0.5$), the compounds can display ferromagnetic, antiferromagnetic, and charge-ordered states, depending on the thermal and magnetic history as well as the preparation conditions (e.g., preparation in oxygen or in air) and temperature.[10,11]

It has been observed that both ferromagnetic and antiferromagnetic transitions are associated with changes in the lattice parameters. The dopant concentration also affects the Mn^{4+}/Mn^{3+} ratio and Jahn−Teller distortions of the MnO_6 octahedron.[12] A number of studies show that the $La_{1-x}Ca_xMnO_3$ perovskite structure is deformed away from the ideal, cubic form, depending on doping levels and synthesis conditions; cubic, tetragonal, orthorhombic, and rhombohedral forms can be synthesized.[6,7,13] However, there is no detailed systematic study available for the $LaMnO_3$−$CaMnO_3$ system to show how lattice parameters change with the La:Ca ratio. The relationship between ionic radii and magnetic properties shows that varying the ionic size of the dopants will change the magnetic properties significantly.[4] Moreover, these are important uncertainties concerning the nature and extent of the cation distribution in the system, which will also strongly affect the electronic and magnetic properties. In the present study, we therefore employ computer simulation methods to calculate the variation of

* To whom correspondence should be addressed. E-mail: javeda@pinstech.org.pk or javed06@hotmail.com (M. J. A.), smw@ri.ac.uk (S. M. W.).
† The Royal Institution of Great Britain.
‡ Pakistan Institute of Nuclear Science and Technology.
§ The Australian National University.

(1) von Helmolt, R.; Wecker, J.; Schulz, B.; Holzapfel, B.; Schultz, L.; Samwer, K. *Phys. Rev. Lett.* **1993**, *71*, 2331.
(2) Schiffer, P.; Ramirez, A. P.; Bao, W.; Cheong, S. W. *Phys. Rev. Lett.* **1995**, *75*, 3336.
(3) Hwang, H. Y.; Cheong, S. W.; Radaelli, P. G.; Marezio, M.; Batlogg, B. *Phys. Rev. Lett.* **1995**, *75*, 914.
(4) Rao, C. N. R.; Mahesh, R.; Raychaudhuri, A. K.; Mahendiran, R. *J. Phys. Chem. Solids* **1996**, *59*, 487.
(5) Shimura, T.; Hayashi, T.; Inaguma, Y.; Itoh, M. *J. Solid State Chem.* **1996**, *124*, 250.
(6) Hibble, S. J.; Cooper, S. P.; Hannon, A. C.; Fawcett, I. D.; Greenblatt, M. *J. Phys. Condens. Matter* **1999**, *11*, 9221.
(7) Rormark, L.; Wiik, K.; Stolen, S.; Grande, T. *J. Mater. Chem.* **2002**, *12*, 1058.
(8) Nadeem, M.; Akhtar, M. J.; Khan, A. Y.; Shaheen, R.; Haque, M. N. *Chem. Phys. Lett.* **2002**, *366*, 433.
(9) Laiho, R.; Lisunov, K. G.; Lahderanta, E.; Petrenko, P. A.; Salminen, J.; Shakhov, M. A.; Safontchik, M. O.; Stamov, V. S.; Shubnikov, M. V.; Zakhvalinskii, V. S. *J. Phys. Condens. Matter* **2002**, *14*, 8043.
(10) Hasanain, S. K.; Shah, W. H.; Akhtar, M. J.; Nadeem, M. *Phys. Rev. B* **2002**, *65*, 144442.
(11) Wang, R.; Mahesh, R.; Itoh, M. *Phys. Rev. B* **1999**, *60*, 14513.
(12) Radelli, P. G.; Cox, D. E.; Marezio, M.; Cheong, S. W.; Schiffer, P. E.; Ramirez, A. P. *Phys. Rev. Lett.* **1995**, *75*, 4488.
(13) Mahesh, R.; Mahendiran, R.; Raychaudhuri, A. K.; Rao, C. N. R. *J. Solid State Chem.* **1995**, *114*, 297.

10.1021/cm052260r CCC: $33.50
Published on Web 02/14/2006

lattice parameters and unit cell volume for $La_{1-x}Ca_xMnO_3$ across the entire series ($x = 0.0-1.0$) and also to predict the distribution of the cations.

Surface properties often play a fundamental role in technological applications, especially in magnetic films. Numerous studies have investigated the surfaces of the colossal magnetoresistance materials.[14−16] The perovskite structure of composition ABO_3 consists of AO and BO_2 atomic layers alternately stacked along the [001] direction. Thus to make a high quality perovskite superlattice, one has to identify and control the surface-terminating layer AO or BO_2. The surface composition of the terminal layer depends on the concentration of the dopant in $La_{1-x}Ca_xMnO_3$; when the Ca concentration is increased, the terminal layers shift from La/Ca to Mn-terminated layers.[16] The terminal layer also depends on the synthesis conditions; when the oxygen pressure is increased, the terminal layer shifts from the MnO_2 plane to that of LaO.[14] The second objective of this study is, therefore, to employ computer simulation techniques to investigate the relative stability of terminal layers in the (010) and (110) surfaces of $LaMnO_3$ and $CaMnO_3$.

Computational Methods

The computer simulation techniques used in the present study are based on an atomistic approach together with lattice energy minimization procedures, a method that has been used to calculate the lattice properties of a number of oxide materials, including $LaMnO_3$.[17−20] These techniques, as well as others for modeling order/disorder in solid solutions, have been reviewed in detail elsewhere.[21−27] We note, however, that (except where we have automated the procedure, see comments below) if a true minimum is not found, which is evident when there is one or more negative phonon frequencies at the Brillouin zone gamma point, the structure is relaxed again after some of the ions are manually displaced in the direction given by the largest components of the corresponding eigenvector.

Our calculations are made on the basis of the Born model of ionic solids with ions assigned integral charges corresponding to their formal oxidation states. The lattice energy is composed of five components: (i) the coulomb term, which is computed using an Ewald summation; (ii) the short-range nondirectional forces between the cations and anions, modeled by Born−Mayer potentials; (iii) short-range anion−anion interactions, modeled by a Buckingham potential; (iv) a driving force for the Jahn−Teller distortions of the coordination sphere of Mn^{3+}, modeled by the inclusion of a ligand field term;[20] and (v) ionic polarization of the oxygen ions, treated by the shell model.

We are particularly interested in modeling the changes in lattice parameters due to variation in the Ca concentration. The full unit cell for the end compositions, or orthorhombic unit cell (where $Z = 4$), contains 20 ions. When solid solutions $La_{1-x}Ca_xMnO_3$ are modeled, the size of this cell restricts the possible values of x to 0, $^1/_4$, $^1/_2$, $^3/_4$, and 1 (assuming full occupancy of sites). For each composition, the lattice energy (and lattice parameters) may depend on how the cations are ordered. In our calculations. we therefore employed a supercell (SC) approach,[28,29] in which the largest configuration examined contained 160 ions ($Z = 32$). Thus we are able to model solid solutions $La_{1-x}Ca_xMnO_3$ where $x = 0$, $^1/_{32}$, $^1/_{16}$, $^3/_{32}$, ..., $^{31}/_{32}$, 1. The number of different ways in which the cations can be ordered depends on both x and Z. So the lowest energy cation distribution obtained for each respective composition (with the exception of $x = 0$ and 1) may change with a larger supercell size. Particular attention is therefore given to compositions $x = ^1/_4$, $^1/_2$, and $^3/_4$, which we are able to model using $Z = 4$ (orthorhombic cell) and $Z = 32$ ($2 \times 2 \times 2$ supercell).

Even with a $2 \times 2 \times 2$ supercell, the number of possible cation-ordered solid solutions, N, to examine is large; ignoring any symmetry

$$N = \left[\frac{n!}{(n-m)!m!}\right]^2$$

where n is the number of A sites in the unit cell and m is the number of La ions. Note the expression is squared, as the number of combinations on the B site is identical to that on the A site. For the $Z = 4$ system, we therefore have $N = 1$, 16, 36, 16, and 1 for $x = 0$, $^1/_4$, $^1/_2$, $^3/_4$, and 1, respectively, whereas for $Z = 32$, we have $N = 1$, 32^2, ..., 361297635242552100, ..., 32^2, and 1 for $x = 0$, $^1/_{32}$, ..., $^1/_2$, ... $^{31}/_{32}$, and 1, respectively. When all A sites (or B sites) are initially equivalent (i.e., starting from one of the end compositions), the lattice energy does not depend on where the first cation is substituted, so there are in fact N/n different configurations to model for compositions $0 < x < 1$. For compositions where N/n is less than 40, we modeled all cation configurations; otherwise, we examined a subset of configurations generated by simulated annealing Monte Carlo (SA-MC), as explained below.

An alternative approach is to use fractional occupancies by employing a mean field (MF) strategy,[30] which aims to model a random distribution of cations. This approach is more appropriate for solid solutions nearer the end compositions and when the cations on equivalent sites are of similar radius, shape, and charge. In the present study, we have also calculated the variation of the lattice parameters in $La_{1-x}Ca_xMnO_3$ using this procedure for $0 < x < 1$. For the respective end compositions there is only one configuration for the cations; the observed structural parameters, which are readily available, are used as the initial structural parameters. For each of the other compositions. the initial structural parameters α_x were obtained by combining the relaxed structural parameters β_x of the end compositions ($x = 0$ and 1)

(14) Yoshimoto, M.; Maruta, H.; Ohnishi, T.; Sasaki, K.; Koinuma, H. *Appl. Phys. Lett*. **1998**, *73*, 187.
(15) Zhang, W.; Wang, X.; Boyd, I. W. *Appl. Phys. Lett*. **1998**, *73*, 2745.
(16) Choi, J.; Zhang, J.; Liou, S. H.; Dowben, P. A.; Plummer, E. W. *Phys. Rev. B* **1999**, *59*, 13453.
(17) Akhtar, M. J.; Waseem, S. *Chem. Phys*. **2001**, *274*, 109.
(18) Shaheen, R.; Akhtar, M. J.; Nadeem, M.; Haque, M. N. *J. Phys. Chem. Solids* **2003**, *64*, 237.
(19) De Souza, R. A.; Islam, M. S.; Tiffee, E. I. *J. Mater. Chem*. **1999**, *9*, 1621.
(20) Woodley, S. M.; Battle, P. D.; Catlow, C. R. A.; Gale, J. D. *J. Phys. Chem. B* **2001**, *105*, 6824.
(21) Catlow, C. R. A. In *Solid State Chemistry*: *Techniques*; Cheetham, A. K., Day, P., Eds.; Clarendon Press: Oxford, U.K., 1987; p 231.
(22) Catlow, C. R. A.; Ackermann, L.; Bell, R. G.; Cora, F.; Gay, D. H.; Nygren, M. A.; Pereira, J. C.; Sastre, G.; Slater, B.; Sinclair, P. E. *Faraday Discuss*. **1997**, *106*, 1.
(23) Allan, N. L.; Mackrodt, W. C. *J. Chem. Soc., Faraday Trans.* **1989**, *85*, 385.
(24) Purton, J. A.; Blundy, J. D.; Taylor, M. B.; Barrera, G. D.; Allan, N. L. *Chem. Commun.* **1998**, *5*, 627.
(25) Purton, J. A.; Barrera, G. D.; Allan, N. L.; Blundy, J. D. *J. Phys. Chem. B* **1998**, *102*, 5202.
(26) Bakken, E.; Allan, N. L.; Barron, T. H. K.; Mohn, C. E.; Todorov, I. T.; Stolen, S. *Phys. Chem. Chem. Phys.* **2003**, *5*, 2237.
(27) Todorov, I. T.; Allan, N. L.; Lavrentiev, M. Y.; Freeman, C. L.; Mohn, C. E.; Purton, J. A. *J. Phys.: Condens. Matter* **2004**, *16*, S2751.
(28) Wahid, F. A.; Thomson, G. B.; Graham, G. M.; Jackson, R. A. *J. Mater. Chem.* **2002**, *12*, 3799.
(29) Leslie, M.; Gillan, M. J. *J. Phys. C: Solid State Phys*. **1985**, *18*, 973.
(30) Morris, B. C.; Flavell, W. R.; Mackrodt, W. C.; Morris, M. A. *J. Mater. Chem*. **1993**, *3*, 1007.

$$\alpha_x = \frac{m\beta_0 + (n-m)\beta_1}{n}.$$

For convenience, we define β_x as the relaxed structural parameter for each composition x obtained in this way.

In our investigations, we also examined how the coulomb interactions would drive the ordering of the cations, but as each configuration would collapse when relaxed without the use of short-range repulsive forces, we chose the structural parameters. For the $Z = 4$ system, we compared the coulomb contribution of the lattice energy for all unique cation configurations for structural parameters α_x and then repeated this procedure using structural parameters β_x. For the $Z = 32$ system, we chose to use the β_x structural parameters, but here we again have a problem of too many unique configurations. In an attempt to find how the cations will order because of differences in the cation charges, we made use of the calculated Madelung potentials (MPs). For example, consider the solid-solution $La_{30}Ca_2Mn_{32}O_{96}$ ($x = {}^1/_{16}$ and $Z = 32$). We initially label all A sites as La with an average charge of 2.9375 and B sites as Mn(III) with an average charge of 3.0625. On the La sublattice, we substitute Ca^{2+} on a site that has the lowest-magnitude MP. Next, on the Mn(III) sublattice, we substitute Mn^{4+} on a site with the highest-magnitude potential, which is continued until the correct numbers of Ca^{2+} and Mn^{4+} ions have been substituted. Note that after each substitution, the charges of the remaining La and Mn(III) ions are adjusted such that the unit cell remains neutral and the MP is recalculated before selecting the next site. When the substitutions are completed, the charge on the remaining La and Mn(III) ions is 3. For each composition, using the structural parameters β_x, the initial MP is different; therefore, this process is repeated from the beginning. However, for compositions in which x is larger than 0.5, the A sites are labeled as Ca ions and the B sites as Mn(IV) ions; La^{3+} and Mn^{3+} ions are substituted on the Ca and Mn(IV) sublattices with the highest and lowest potentials, respectively. We note that this procedure[31] does not guarantee that we find the most-stable configurations, but we will find one of the lower-energy configurations, which we then choose to use as the initial starting configurations in our Monte Carlo (MC) calculations.

To explore the possibility of lower-energy arrangements in the larger supercells, we have used a global optimization algorithm, MC, to search the configurational space. The MC calculations use a library of simple routines that we have derived to exploit the large numbers of loosely coupled computers becoming available via the use of grid technologies. We presume that the relaxation of the lattice parameters β_x (for any explicit cation order) requires, on average, less CPU effort than if we had chosen α_x. The search algorithm is as follows: (1) Perform an energy minimization of the initial structure in which both the atomic coordinates and cell parameters are relaxed. Store the final total lattice energy. (2) Randomly exchange atoms within the A or B sites with equal (50%) probability. (3) If the A site is selected, choose a random Ca atom and a random La atom with equal probability; otherwise, select a random Mn(III) and a random Mn(IV) atom on the B site. (4) Exchange the pair of selected ions and minimize the energy of the structure (again, cell parameters and atomic coordinates are relaxed). Store the lattice energy. (5) Accept or reject the exchange using the Metropolis algorithm,[32,33] and return to step 2. Note that the relaxed structure is never used as the initial structural parameter for the next energy minimization and all minimizations are initialized from the charge-ordered structures with exchanged atoms. To guide the exchange Monte Carlo search toward a low-energy configuration, we utilize simulated annealing,[34] whereby the fictitious temperature in the Metropolis algorithm decreases so that the rate of exchange acceptance falls from 50% exchange acceptance at the start of the run to 5% exchange acceptance at the end.

The general utility lattice program (GULP),[35] which was modified to allow partial occupancies within the ligand-field contribution to the lattice energy, was used for all the bulk calculations. An additional script, containing the Monte Carlo routines, was used to automate the iterative process of reading the latest GULP output file, the generation of the next GULP input file, and submission of the GULP job.

For atomistic calculations of surface structures, the most commonly used approach is to employ 2D periodic boundary conditions for planes parallel to the surface of the material. Perpendicular to the plane of the surface, the simulation block is divided into two regions: the near surface region, where atoms adjacent to the surface or interface are allowed to relax to their minimum energy configuration, and a the more distant region, where ions are held fixed at their bulk equilibrium positions. The simulations, and thus any predictions, operate on the assumption that the surface is created or grown in a vacuum. Note that the partial pressure of oxygen, for example, is likely to strongly influence the composition and electronic structure of the external surface. For the calculation of surface energies, we have employed the MARVIN code.[36] The potential model used in the study of surface calculations omits ligand-field effects, because MARVIN does not currently implement the ligand-field potential. However, we expect surface relaxation to be dominated by monopolar and dipolar electrostatic interactions and note that the shell-model potential, without ligand-field terms, gives a reasonable structure for the crystal bulk.

Results and Discussions

Bulk Simulations. The success of computer simulations depends on the quality and transferability of potential parameters used. In the present study, we use previously derived potential parameters, which, for $CaMnO_3$, are those fitted to reproduce the lattice parameters of respective binary oxides.[37] $CaMnO_3$ contains spherical ions, whereas in $LaMnO_3$, the Mn(III) is an open-shell ion; therefore, the potential parameters for $LaMnO_3$ include ligand-field effects, which are essential in modeling the distorted MnO_6 octahedron.[20,38] All parameters are presented in Table 1. In Table

(31) Occasionally, we were able to find a lower-energy configuration by examining the "final" MP. For example, for $LaCa_3Mn_4O_{12}$ ($Z = 32$), we changed back the La with the highest MP (which was not the last La to be placed) to a Ca (and similarly for a Mn^{3+}) and then recalculated the MP and found a better site (lower MP) for the La (and Mn^{3+}). On further investigation, we found that the rogue positioning of the La (and consequently the next Mn^{3+}) occurred when placing the 7th La ion. At this point, of the remaining A sites containing Ca ions, there were four sites with the lowest MP, a pair of rogue sites with a slightly lower MP than that of the two sites, which would lead to the lowest-found energy configuration. Interestingly, had we placed the 7th Mn^{3+} first, the rogue Mn^{3+} sites (although still with a MP similar to that of our preferred sites) would not have been selected.

(32) Metropolis, N.; Ulam, S. *J. Am. Stat. Assoc.* **1949**, *44*, 335.
(33) Allen, M. P.; Tildesley, D. J. *Computer Simulation of Liquids*; Oxford University Press: Oxford, U.K., 1986.
(34) Kirkpatrick, C. D.; Gelatt, C. D., Jr.; Vecchi, M. P. *Science* **1983**, *220*, 671.
(35) Gale, J. D. *J. Chem. Soc., Faraday Trans.* **1997**, *93*, 629.
(36) Gay, D. H.; Rohl, A. L. *J. Chem. Soc., Faraday Trans.* **1995**, *91*, 925.
(37) Woodley, S. M.; Battle, P. D.; Gale, J. D.; Catlow, C. R. A. *Phys. Chem. Chem. Phys.* **1999**, *1*, 2535.
(38) Woodley, S. M.; Catlow, C. R. A.; Gale, J. D.; Battle, P. D. *Chem. Commun.* **2000**, *19*, 1879.

Table 1. Potentials Parameters Used for $La_{1-x}Ca_xMnO_3$[a]

(i) $A\exp^{(-r/\rho)} - Cr^{-6}$ (potential cutoff = 12 Å)			
interaction	A (eV)	ρ (Å)	C (eV Å^6)
$La^{3+}-O^{2-}$	4317.17	0.2987	0.0
$Mn^{3+}-O^{2-}$	1265.17	0.3176	0.0
$Mn^{4+}-O^{2-}$	3329.39	0.2642	0.0
$Ca^{2+}-O^{2-}$	2272.74	0.2986	0.0
$O^{2-}-O^{2-}$	25.41	0.6937	32.32
$Mn_{LF}{}^{3+}-O_{LF}{}^{2-}$	8.98	0.3300	

(ii) Shell Model		
species	charge on shell (e)	spring constant (eV Å^2)
O^{2-}	−2.513	20.53

[a] r is the interatomic distance and the subscript LF indicates that the parameters form part of the ligand-field term.[20]

Table 2. Comparison of Calculated and Experimental Structural Data for $LaMnO_3$ and $CaMnO_3$

	$LaMnO_3$			$CaMnO_3$		
params	calcd	exp[39]	% error	calcd	exp[40]	% error
a (Å)	5.7483	5.7430	0.09	5.2637	5.2790	−0.29
b (Å)	7.7204	7.6950	0.33	7.4441	7.4600	−0.21
c (Å)	5.5301	5.5370	−0.12	5.2638	5.2730	−0.17
V (Å^3)	245.42	244.69	0.30	206.25	207.66	−0.68

2, we compare the calculated and experimental structural data for $LaMnO_3$[39] and $CaMnO_3$[40] along with the percentage discrepancies between our calculated models and experimental results. We note that the calculated structures have less than 0.70% error compared to the experimentally observed data, which indicates the reliability of our potential model for both end compositions. We can therefore be confident that these potentials are applicable for intermediate compositions. The calculated lattice energy is −27.81 eV/atom for $LaMnO_3$ and −32.45 eV/atom for $CaMnO_3$.

Heat of Mixing and Unit Cell Dimensions. The variations in the lattice energy as a function of composition, defined when using the MF approach and for the predicted ground-state found using the MC approach, are shown in Figure 1a. For each composition x, the lowest lattice energy for $La_{1-x}Ca_xMnO_3$ was obtained when the cations were ordered on both the A and B sites, which is to be expected because there are fewer degrees of freedom when the MF approach for $La_{1-x}Ca_xMnO_3$ (when $0 < x < 1$) is applied. The heat of mixing, $\Delta U(x)$, for different concentrations of Ca in the host lattice is defined as follows

$$\Delta U = U_{(La_{1-x}Ca_xMnO_3)} - (1-x)U_{(LaMnO_3)} - xU_{(CaMnO_3)}$$

where $U_{(La_{1-x}Ca_xMnO_3)}$, $U_{(CaMnO_3)}$, and $U_{(LaMnO_3)}$ are the lattice energies of the intermediate composition (doped system), pure $CaMnO_3$, and pure $LaMnO_3$, respectively. From Figure 1b, it is clear that $|\Delta U(x)|$ for the ordered structures has a maximum at $x = {}^1/_2$ and that either side the variation is almost linear; although we may not have found the lowest-energy configurations, especially near $x = {}^1/_2$. As the heat of mixing is always negative (i.e., exothermic), our calculations suggest that there will be formation of a continuous solid solution.

(39) Elemans, J. B. A. A.; van Laar, B.; van der Veenm, K. R.; Loopstra, B. O. *J. Solid State Chem.* **1971**, *3*, 238.
(40) Jorge, M. E. M.; dos Santos, A. C.; Nunes, M. R. *Int. J. Inorg. Mater.* **2001**, *3*, 915.

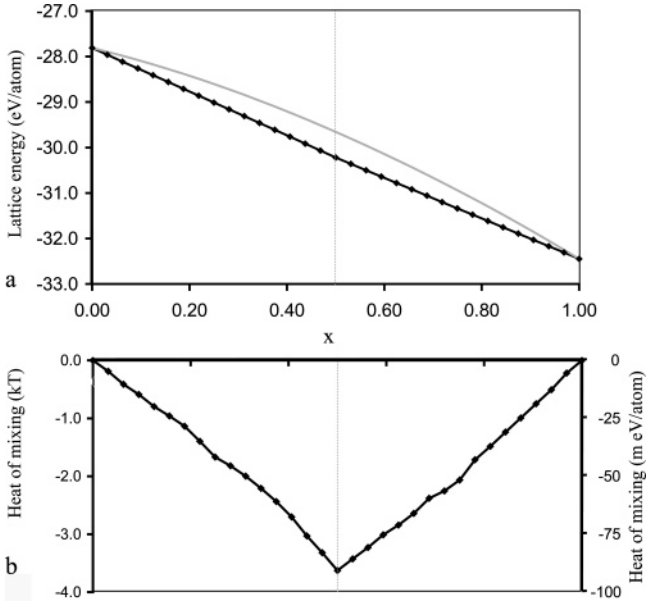

Figure 1. Calculated (a) lattice energy and (b) heat of mixing (at room temperature) in $La_{1-x}Ca_xMnO_3$ for the cation-ordered, ground-state (black points and line) data and when the MF approach was used (gray line).

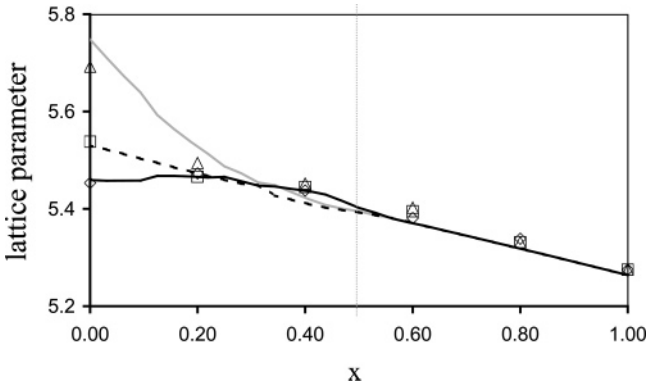

Figure 2. Calculated variations of lattice parameters with Ca concentration in $La_{1-x}Ca_xMnO_3$, $Z = 32$, using a MF approach (lines) and experimental data[7] (symbols): a (Å, gray line and triangles), $b/\sqrt{2}$ (Å, black line and diamonds), c (Å, broken line and squares).

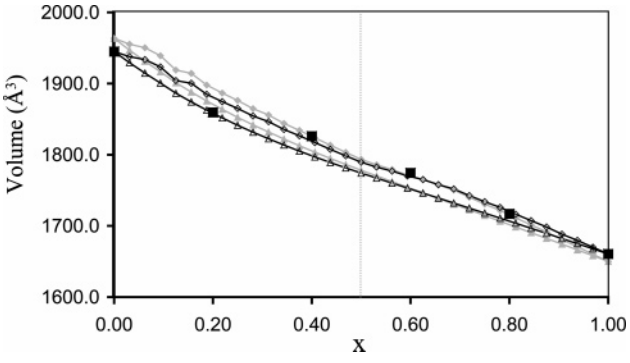

Figure 3. Calculated variations of the $Z = 32$ unit cell volume (Å^3) with Ca concentration in $La_{1-x}Ca_xMnO_3$: that which employs a MF approach (triangles) and those for the charge-ordered ground state (diamonds)[1] and experimental (solid squares) values. Darker line indicates rescaled data, $V'(x)$, and lighter line indicates original data, $V(x)$.

Figures 2−4 show the variations of the unit cell volumes and lattice parameters with Ca doping in $La_{1-x}Ca_xMnO_3$, for which our calculated results are compared with the experimental data.[7] We note that there are two popular choices when labeling the lattice parameters a, b, and c.[6,7] Where necessary, experimental data have been converted, for ease

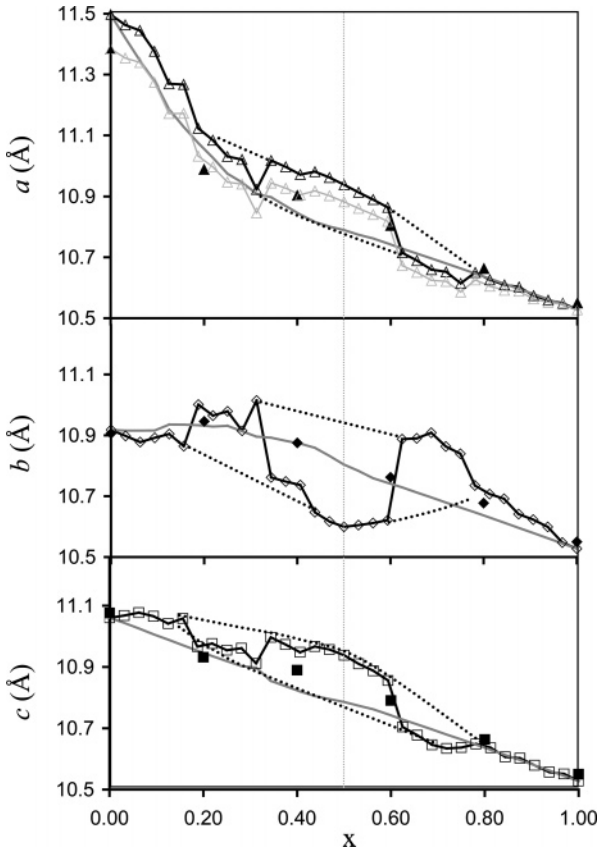

Figure 4. Calculated variations of the lattice parameters with Ca concentration in $La_{1-x}Ca_xMnO_3$, $Z = 32$: that which employs a MF approach (gray lines) and those for for the charge-ordered, ground-state (open symbols) and experimental (solid symbols) values. The open triangles on a lighter line indicate rescaled data, $a'(x)$, and the darker line with open triangles indicates original data, $a(x)$.

of comparison, so that *a* is always greater than *c*. Somewhat surprisingly, the predicted unit cell volumes for the cation-ordered, ground-state structures are larger than those predicted when the MF approach (random cation distribution) is employed (see Figure 3). Presumably, the expansion of the cell with explicit doping, with respect to MF, occurs because MF distortions tend to average one another out, whereas with explicit atoms, doping causes local and nonlocal distortions.

If we assume the cations are randomly distributed on the A and B sites, unlike the ordered structures, we predict a smooth and continuous variation in the lattice parameters with respect to *x*, the relative concentration of Ca in the host lattice. Our calculated lattice parameters are in good agreement with those observed,[7] as shown in Figure 2, where both sets of data are overlaid. From Figure 2, it is also clear that our relaxed simulation cell remains orthorhombic when there are higher concentrations of La and Mn(III); $(1 - x) > {}^1/_2$. For higher concentrations of Ca and Mn(IV), the relaxed simulation cell becomes tetragonal for $0.5 < x < 0.65$ and cubic for $x > 0.65$.

Our predicted variations of the unit cell volume for ordered-cation, ground state distributions (with the exception of the 20% Ca doping) are in good agreement with experimental observations and appreciably better than those predicted using the MF approach (i.e., when a random distribution of cations is modeled), as shown in Figure 3. Here, we show both the raw data ($V(x)$, gray line) and that after a linear rescaling

$$V'(x) = V(x) - x(V(1) - V_{obs}(1)) - (1 - x)(V(0) - V_{obs}(0))$$

so that the discrepancies in the predicted and observed unit cell volume for the end members are removed.

On the basis of the raw data shown in Figure 4, it would appear that the difference in the observed and predicted volumes for the charge-ordered 20% Ca-doped structure is due to our simulated structures having a larger *a* parameter (and to a lesser extent, larger *b* and *c* parameters) than that reported in ref 7. We note though, that there is a similar discrepancy between observed values reported for the *a* parameter for the pure $LaMnO_3$ phase; ref 39 reports *a* ($Z = 4$) as 5.743 Å, whereas it is reported here, and shown in Figure 4a, as 5.692 Å. As there is a smaller and, moreover, similar discrepancy in *a*, *b*, and *c* parameters for the pure $CaMnO_3$ phase, we also show the rescaled data (gray triangles and line in Figure 4a).

$$a'(x) = a(x) - (1 - x)(a(0) - a_{obs}(0))$$

The difference in a' and a_{obs} for the 20% Ca composition is quite small and not larger than that seen in *b* and *c*. Moreover, $a'(x)$ agrees very well, and much better than $a(x)$, with the observed *a* values for 40 and 60% Ca compositions.

The discrepancy around $x = 0.2$ that still exists between V' and that observed could be due to the nonstoichiometric nature of pure and 20% Ca-doped samples, whereas other compositions are reported to be stoichiometric.[7] It appears, therefore, that for stoichiometric systems, there is a linear decrease in the lattice parameters with an increase in the Ca concentration, as might be expected. However, our study clearly shows that the compressibility of the *a* parameter is larger than that of the *c* parameter. Above 35% Ca concentration, the orthorhombic splitting is suppressed, with $a \cong c$, indicating tetragonal symmetry, in agreement with previous experimental observations.[41]

As evident in Figure 4, when the cations are ordered, oscillations appear in our predicted lattice parameters for the ground-state structures with composition $0.2 < x < 0.8$. The oscillations that occur in the *a* and *c* lattice parameters have a smaller amplitude and are antiphase to the oscillations in the *b* lattice parameter. Thus the variation of the unit cell volume with respect to Ca doping does not contain any significant oscillations.

As discussed above, the number of different ways the cations can order is dependent upon the value of *x* (as well as *Z*). In particular, this configurational space is much larger for values of *x* near ${}^1/_2$. Indeed, early results from the MC runs showed a higher frequency of oscillations of the lattice parameters (for the best ground state so far found) between two extreme curves (shown as dotted black lines in Figure 4), caused by insufficient sampling of the configurational space. More rapid oscillations were removed by continuing the MC runs, and in particular by seeding the MC runs with the ground-state configurations found for neighboring com-

(41) Hasanain, S. K.; Nadeem, M.; Shah, W. H.; Akhtar, M. J.; Hasan, M. M. *J. Phys. Condens. Matter* **2000**, *12*, 9007.

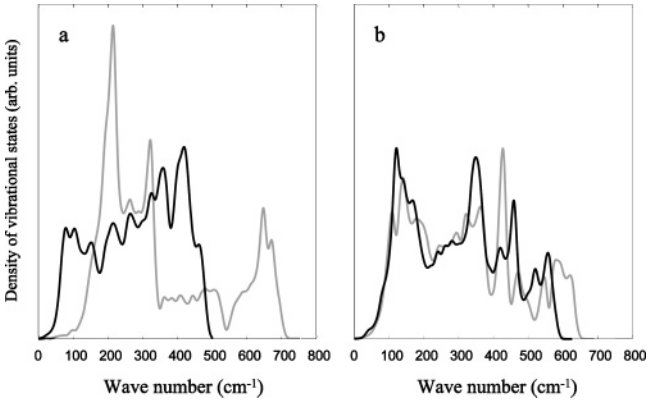

Figure 5. Calculated density of states for (a) the end compositions of $LaMnO_3$ (darker line) and $CaMnO_3$ and (b) for a random (using a MF approach) and ordered (darker line) arrangement of the cations in $LaCaMn_2O_6$.

positions (and then adjusting the composition of cations by randomly selecting one A cation and one B cation to change), than by using the structural parameters β_x. We found that certain cation-ordered structures could be found with lattice energies similar to that of the ground state but with structural parameters that lie close to the opposite extreme (dotted black line, Figure 4). Thus a statistical treatment of these configurations for each of the compositions $0.2 < x < 0.8$ would probably predict "average" lattice parameters that are nearer the observed values.

A general decrease in the lattice parameters with Ca concentration is expected. The ionic radii of the La^{3+} and Ca^{2+} ions with a coordination number (CN) of 12 are 1.36 and 1.34 Å, respectively.[42] It has been noted before that because of Ca^{2+} doping at the La^{3+} sites, an equivalent amount of Mn^{3+} is converted into Mn^{4+} to maintain the electroneutrality of the system. The ionic radii of Mn^{3+} and Mn^{4+} are 0.58 and 0.53 Å, respectively;[42] therefore, it is expected that lattice parameters and unit cell volume decrease as the Ca concentration increases. For $LaMnO_3$, the calculated density of 6.54 g/cm^3 is in good agreement with the experimental[43] value of 6.57 g/cm^3. The calculated bulk modulus for $CaMnO_3$ (325.38 GPa) is much larger than that of $LaMnO_3$ (135.19 GPa), which shows it is more difficult to compress $CaMnO_3$ than $LaMnO_3$.

Lattice Dynamics. To determine the vibrational properties of the $La_{1-x}Ca_xMnO_3$ system, we have calculated the phonon density of states for $x = 0$, $^1/_2$, and 1, as presented in Figure 5. For $LaMnO_3$, the intensity of peaks is evenly distributed between a frequency range of 50 and 500 cm^{-1}. In contrast, for $CaMnO_3$, although there is a wider range of frequency (up to 700 cm^{-1}), there are two compressed regions of dispersion bands, one between 180 and 350 cm^{-1} and another higher in energy between 600 and 700 cm^{-1}. In addition, $LaMnO_3$ has softer acoustic bands than $CaMnO_3$; the edge of the first peak is about 100 cm^{-1} lower. We note that the first peaks contain the breathing modes of the Jahn−Teller distortion in the MnO_6 octahedra.

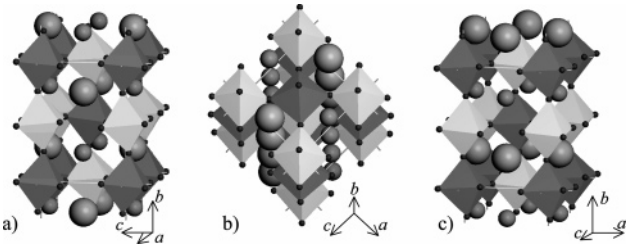

Figure 6. Different cation-ordered structures for $LaCaMn_2O_6$ within an orthorhombic unit cell ($Z = 4$), in which the lighter/darker octahedra contain Mn(III)/Mn(IV) ions, respectively, and the largest spheres represent the La(III) ions.

These results clearly indicate that the lattice vibrational properties will change on varying the La:Ca ratio. Indeed, in Figure 5b, where we present the vibrational density of states calculated assuming a random and then ordered arrangement of cations (with $Z = 4$) for the solid solution $x = {}^1/_2$, we see that there are significant changes in the profile of the density of states and thus significant movement of the phonon bands. For both calculations, the frequency ranges of the phonon bands are bound by that calculated for the end compositions.

The density of states profile is also strongly dependent on the cation distribution, the most noticeable difference being that the smaller range of frequencies for the random arrangement of cations and the intensity for the two peaks near 450 cm^{-1} are reversed. When a MF approximation is used to model a random arrangement cations, the structural relaxation about the A sites is similar to that of a spherical ion with an average La:Ca ionic radius, whereas for the B sites, there is also a competing Jahn−Teller response between Mn^{3+} and Mn^{4+} ions. We consider that the latter is the most likely source of the disparity between the two profiles.

Cation Order. It is helpful to visualize the perovskite crystal structure as two separate interpenetrating simple cubic sublattices with lattice axes *ac*, −*ac*, and *b*; *ac* planes of corner-sharing BO_6 octahedra stacked in the *b* direction and a simple cubic lattice of spherical A cations. The MnO_6 are generally distorted such that there are three unique Mn−O bond lengths, short and long within *ac* layers and medium-length bonds connecting the *ac* layers. The oxygen anions forming the medium-length bonds with the manganese(III) ions occupy the same *ac* plane as that occupied by the A cations.

For $Z = 4$, we were able to perform an exhaustive search for three solid solutions, $x = {}^1/_4$, $^1/_2$, and $^3/_4$. $La_2Ca_2Mn_4O_{12}$ provides the most interesting case in that there are more possible cation configurations. If we consider only the coulomb contributions to the lattice energy, we find that both the A and B sublattices form a checkered pattern within *ac* layers and with cations alternating ($La^{3+}-Ca^{2+}-La^{3+}$ or $Mn^{4+}-Mn^{3+}-Mn^{4+}$) along the *b* axis (thus the other two principle planes of the simple cubic sublattices, (*ac*)*b* and (−*ac*)*b*, are also checkered). This configuration is shown in Figure 6a. Relaxation of lattice parameters α_x and β_x leads to two different cation ordering schemes on the A sublattice that had a lower lattice energy. In one of these, the La^{3+} and Ca^{2+} ions are still checkered in the *ac* layers, but along the *b* direction, these cations no longer alternate, as shown

(42) D. R. Lide, Ed. *CRC Handbook of Chemistry and Physics*, 83rd ed.; CRC Press: Boca Raton, FL, 2002−2003; pp 12−14.
(43) van Roosmalen, J. A. M.; Cordfunke, E. H. P. *J. Solid State Chem.* **1994**, *110*, 106.

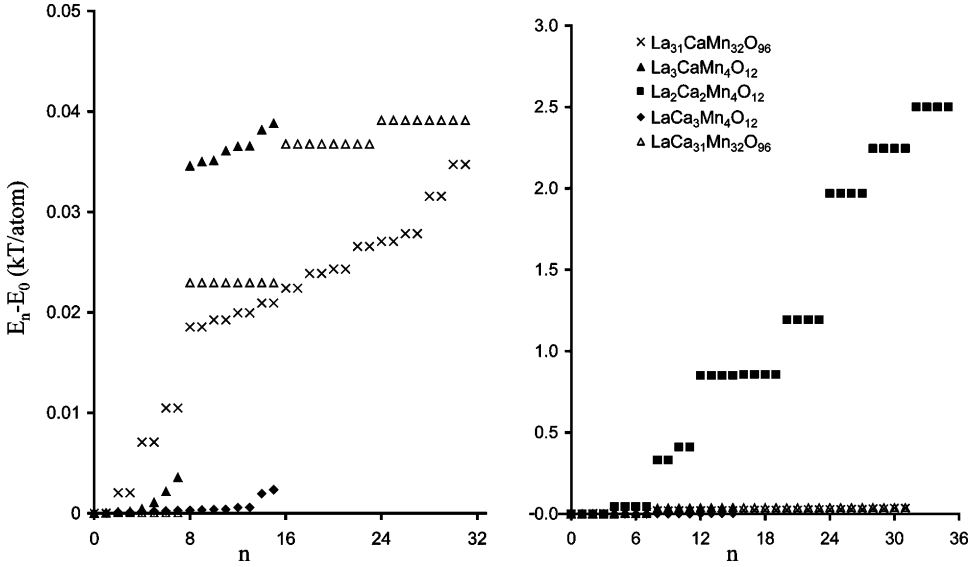

Figure 7. Calculated relative lattice energies for all possible charge-ordered configurations for compositions $x = {}^1/_4$, ${}^1/_2$, and ${}^3/_4$ where $Z = 4$ and for compositions $x = {}^1/_{32}$ and ${}^{31}/_{32}$ where $Z = 32$.

in Figure 6b. The lowest-energy configuration contained *ac* layers of La^{3+} ions, which alternate with *ac* layers of Ca^{2+} ions, as shown in Figure 6c. Note that the perovskite structure is composed of corner-sharing MnO_6 octahedra, with the remaining cations filling the A site holes. Ignoring any distortions, the difference in the ionic radii for the B site cations is much larger than that for the A site cations. Thus one might have erroneously expected that the size effects would change the ordering of the octahedra (B sites) and that coulomb effects would determine the A site cation order.

For $LaCa_3Mn_4O_{12}$ ($Z = 4$), it is convenient to consider first the system in which the ions have the same fractional coordinates as that of the cubic phase, but in which we maintain the orthorhombic cell. Provided that $a \neq c$, there are two unique configurations: the La and Mn^{3+} ions within the same *ab* plane or within the same *bc* plane, depending on whether the La and Mn^{3+} are as close or as far away as possible. The interatomic distance is either

$$\sqrt{\frac{a^2}{4} + \frac{b^2}{16}}$$

or

$$\sqrt{\frac{b^2}{16} + \frac{c^2}{4}}$$

respectively. We find that coulomb contribution to the lattice energy suggests that La and Mn^{3+} should be as close to each other as possible. When the octahedra are rotated, one of the originally longest A−B interatomic distances becomes the shortest A−B interatomic distance. Even so, the same cation configuration is found, i.e., the La and Mn^{3+} are approximately within the same *bc* plane, where $c < a$, as the average distances should be considered. The equivalent result is found for $La_3CaMn_4O_{12}$ ($Z = 4$): the coulomb contribution to the lattice energy suggests that the Ca and Mn^{4+} should be as close to each other as possible. When the lattice energy of each relaxed structure is considered, we find that the cation configuration changes for $La_3CaMn_4O_{12}$, whereas the difference in the lattice energy is quite small for $LaCa_3Mn_4O_{12}$, as $a \approx c$.

For $Z = 32$, we performed an exhaustive search of the possible cation ordering for $La_{31}CaMn_{32}O_{96}$ ($x = {}^1/_{31}$) and $LaCa_{31}Mn_{32}O_{96}$ ($x = {}^{31}/_{32}$). For the $x = {}^{31}/_{32}$ composition, the calculations of both the coulomb contribution (before relaxation) and the lattice energy (after relaxation) suggest that the La^{3+} and Mn^{3+} ions once more are as close as possible to each other. The La^{3+} ion occupies the center of a Mn_8 cube; therefore, there are eight equivalent sites for the Mn^{3+} ion (once the location of the La^{3+} has been chosen). For the $x = {}^1/_{32}$ composition, a similar result is found when the coulomb contributions are considered; the Ca^{2+} and Mn^{4+} ions are as close as possible to each other. However, the lattice-energy calculations predict that the Mn^{4+} ion occupies the next-nearest B site in the *ac* plane that contains the B sites nearest to the calcium ion. Again, there are eight equivalent configurations once the cation order on the A sublattice has been decided.

Clearly, a higher La:Ca ratio (and therefore a greater content of the nonspherical Mn^{3+} ion) leads to an enhanced possibility that a different cation distribution will be predicted to be the most stable, when considering only the charges and when the lattice energy is fully minimized. Thus we would expect that initializing our MC calculations with a cation order suggested by considering the MP for the various configurations will probably prove more successful for solid solutions with a higher content of Ca (larger value of x).

For each composition ($x = {}^1/_4$, ${}^1/_2$, and ${}^3/_4$) that can be modeled within the $Z = 4$ unit cell, no lower-energy configuration was found when the MC technique was used to sample different possible cation ordering within the $Z = 32$ unit cell. Although we were not able to search the entire configurational space for $Z = 32$, it should be noted that the predicted ground-state cation order might change if a larger value of Z is used.

The lattice energies per atom for all possible configurations for compositions $Z = 4$ ($x = {}^1/_4$, ${}^1/_2$, and ${}^3/_4$) and $Z = 32$ ($x = {}^1/_{32}$ and ${}^{31}/_{32}$) are shown in Figure 7. For convenience, we

Table 3. Calculated Relaxed Surface Energies (Jm^{-2}) for $LaMnO_3$ and $CaMnO_3$

	$LaMnO_3$		$CaMnO_3$	
Miller index	La-terminated	Mn-terminated	Ca-terminated	Mn-terminated
(010)	1.21	0.94	0.97	1.07
(110)	1.20	0.77	0.63	1.60

have chosen to rescale our data by k_BT, where T is room temperature, i.e., $k_BT = 0.025$ eV. By an order of magnitude, the largest spread in ordering energies exists for $LaCaMn_2O_6$ (see Figure 7b), and the driving force for cation ordering is also likely to be stronger for compositions near $x = {}^1/_2$. However, even for composition $x = {}^1/_2$ at room temperature (which is much lower than typically required during synthesis), there are at least six possible cation distributions with lattice energies that are less than the thermal energy per atom of $2k_BT$ above the ground state. Thus provided the ground-state configurations are included in Figure 7, clearly the distributions of energies shown, particularly in Figure 7a, suggest that the cations in the respective solid solutions are randomly distributed on the A and B sites. Moreover, during the MC runs, the difference between the ground state and the second-lowest-energy configuration found for each composition was less than one thermal energy (at room temperature) per atom and had a maximum at $x = {}^1/_2$.

Surface Simulations. Although there is a considerable body of literature concerned with the determination of the surface structure of $La_{1-x}Ca_xMnO_3$,[14−16] there appears to be little published data on the end compositions $LaMnO_3$ and $CaMnO_3$. As part of a concerted and systematic effort to resolve the surface composition of the $La_{1-x}Ca_xMnO_3$ series, we report here a study of the most widely studied surfaces ((010) and (110)) of the two end compositions $LaMnO_3$ and $CaMnO_3$. Following our earlier discussion, we recall that the surface structure is typically terminated with AO or BO_2; that is, LaO or CaO, or MnO_2. The composition of the perovskite, as has been shown previously,[44] is such that, to achieve the condition of zero net dipole perpendicular to the surface, the configuration must be reconstructed to ensure convergence of the total energy and hence the surface energy. We use this latter criterion to discriminate between the lowest-energy terminations for each given face. The termination with the lowest surface energy is expected to dominate the surface structure at moderate temperature. When the energy difference between two or more different terminations is comparable to k_BT, or if the configurational entropy of terminating structures becomes significant, the structure of the surface is expected to be more complex.

Calculated surface energies for the $LaMnO_3$ and $CaMnO_3$ compositions are shown in Table 3. For each material and each crystal face, different terminating structures were considered on the basis of cleaving the crystal at different positions within a repeated layer. In the case of the (110) face of $LaMnO_3$, one of the Mn-terminated configurations was initially reconstructed to remove a dipole by removing a partial layer of oxygen, which gave rise to the most-stable surface structure. In all other cases, the condition of apolarity perpendicular to the surface was satisfied by terminating the structures with complete layers of either La or Mn (in the case of $LaMnO_3$) or, similarly, Ca or Mn in the case of $CaMnO_3$. For $LaMnO_3$, we predict that both the (010) and (110) surfaces are Mn-terminated, whereas for $CaMnO_3$, we predict Ca termination. It is clear that the terminating species for each end composition of the $La_{1-x}Ca_xMnO_3$ series is different, and hence we expect that the surface structure and properties of the intermediate compositions will depend strongly on the exact Ca concentration and that the terminating species will be sensitive to the La:Ca ratio.

We suggest that the different terminating species arise because the driving force originates from two distinct phenomena. In $LaMnO_3$, the cations are equal in charge but the La^{3+} cation is substantially larger than the Mn^{3+} cation. The smaller Mn cation is more able to maximize coordination with neighboring oxygen atoms at the surface, whereas the large La cation is more constrained and is less stable at the surface. In $CaMnO_3$, the charge on the Ca^{2+} ion is of course smaller than that on the Mn^{4+} ion, though as noted earlier, the Ca ionic radius is larger than that of the Mn species. However, the Mn−O ionic bonds are significantly stronger because of the higher charge of the manganese ion. In this case, it is more favorable to reduce the coordination number of Ca to 8 at the surface, in comparison to 12 in the bulk, than to force the Mn ion to deviate from its ideal coordination state of 6, resulting in the Ca-terminated structure. This argument is supported by previous observations and interpretations in work on perovskite surfaces by Mackrodt[45] and Hines et al.[46]

A point of interest is that the initially Mn-terminated (110) surface undergoes very substantial relaxation, in which three La ions are promoted to the external surface from the subsurface. The relaxed structure exhibits an accessible surface that is dominated by Mn and oxide ions but also contains La ions with incomplete coordination shells. The study described here reports only static structures, and hence future modeling should consider annealing methods to locate or validate surface-structure global minima. We also expect that the relaxation and hence termination of the surface will be strongly influenced by the partial pressure of oxygen in the synthesis environment.

Conclusions

Our computer simulation study has shown that interatomic potential methods are applicable for modeling the entire $LaMnO_3$−$CaMnO_3$ solid solution. The calculated decrease in the lattice parameters with Ca concentration is in good agreement with experimental observations for stoichiometric samples. However, anomalies are observed for nonstoichiometric materials, particularly for 20% Ca-doped samples. Our calculations predict that the decrease in the a parameter with Ca concentration is larger than that of the c parameter, and above a 35% Ca doping level, $a \cong c$, indicating tetragonal symmetry. We have also calculated the phonon density of

(44) Read, M. S. D.; Islam, M. S.; Watson, G. W.; King, F.; Hancock, F. E.; *J. Mater. Chem.* **2000**, *10*, 2298.

(45) Mackrodt, W. C. *Phys. Chem. Miner.* **1988**, *15*, 228.

(46) Hines, R. I.; Allan, N. L.; Flavell, W. R. *J. Chem. Soc., Faraday Trans.* **1996**, *92*, 2057.

states for the two end compositions and $LaCaMn_2O_6$ and find that the phonon bands depend on both x, or the La:Ca ratio, and how the cations are arranged.

For structures in which the concentration of Jahn−Teller Mn(III) ions is greater, we found a greater rearrangement of the Ca and La ions on the A sites, due to steric affects, than that suggested by minimizing the energy contributions from the Madelung field. For example, the Madelung field and lattice-energy calculations (where $Z = 32$) suggest the same arrangement, smallest distance between A site dopant and B site dopant, when the La:Ca cation ratio is 1:31. Conversely, for the 31:1 case, the Madelung field and lattice-energy search results gave different arrangements. When we completed an exhaustive search (where Z and x are fixed), we found that steric affects caused no changes to the cation distribution on the B site (the ground states contained the largest coulomb contributions to the lattice energy). No lower-energy-configuration arrangement of cations was found within the $Z = 32$ cell that could not be modeled within the $Z = 4$ cell. Although we did not attempt to search the entire configurational space for $Z = 32$ or to model more complex cation configurations for $Z > 32$, it does appears that at temperatures where high-temperature synthesis normally occurs, the ordering of the cations is random. However, if a low-temperature route for synthesis can be found, particularly for compositions nearer $x = {}^1/_2$, there may be a sufficient driving force for ordering on both the A and B sites. Currently, we are collecting data so that we may report a statistical treatment of the heat of mixing and structural parameters of $La_{1-x}Ca_xMnO_3$.

From the calculation of surface energies we can conclude that, in $LaMnO_3$ for both the (010) and (110) surfaces, Mn-terminated layers are more stable, whereas in the case of $CaMnO_3$, the Ca-terminated surfaces are more energetically favorable than the Mn-terminated layers. For both end compositions, two distinct driving forces are responsible for the terminating species observed at the surface. And although the results do not allow us to forecast the surface structure at an arbitrary concentration, particularly with static lattice methods, the fact that different species are observed at the surface for the two end compositions indicates that the surface structure is a function of the La:Ca ratio. We are currently pursuing a study of the surface structure at intermediate compositions.

Acknowledgment. M.J.A. thanks the Ministry of Science and Technology, Government of Pakistan, for the award of a postdoctoral fellowship at the Royal Institution of Great Britain, London. We are grateful to EPSRC for the funding of computational resources at the Royal Institution.

CM052260R